



Novel Operating Modes for the Charging of Lithium-ion Batteries

Marc D. Berliner,¹ Benben Jiang,² Daniel A. Cogswell,¹ Martin Z. Bazant,¹ and Richard D. Braatz^{1,z}

¹Massachusetts Institute of Technology, Cambridge, Massachusetts 02139, United States of America

²Tsinghua University, Beijing, People's Republic of China

Conventional battery simulation tools offer current, voltage, and power operating modes. This article presents General Operating Modes (GOMs), which move beyond these standard modes and allow battery models of any scale to simulate novel operating modes such as constant temperature, constant lithium plating overpotential, and constant concentration. The governing equations of the battery model are solved alongside a single algebraic constraint that determines the current. The operating modes are simulated efficiently and deterministically inside a differential-algebraic equation (DAE) solver, and constraints are satisfied within solver tolerances. We propose a mixed-continuous discrete (aka hybrid) solution to the constrained charging problem, using the GOMs to satisfy charging constraints. This approach enables nonlinear model predictive control (NMPC) to be implementable in real-time while directly using sophisticated physics-based battery models. The approach is demonstrated for three models of various complexity: a thin-film nickel hydroxide electrode model, a Single-Particle (SP) model, and a Porous Electrode Theory (PET) model. The hybrid fast charging algorithm is shown to be slightly suboptimal for the thermal SP model in some cases, which is not of practical importance for NMPC.

© 2022 The Author(s). Published on behalf of The Electrochemical Society by IOP Publishing Limited. This is an open access article distributed under the terms of the Creative Commons Attribution Non-Commercial No Derivatives 4.0 License (CC BY-NC-ND, <http://creativecommons.org/licenses/by-nc-nd/4.0/>), which permits non-commercial reuse, distribution, and reproduction in any medium, provided the original work is not changed in any way and is properly cited. For permission for commercial reuse, please email: permissions@iopublishing.org. [DOI: [10.1149/1945-7111/ac9a80](https://doi.org/10.1149/1945-7111/ac9a80)]



Manuscript submitted June 18, 2022; revised manuscript received September 7, 2022. Published October 27, 2022.

Lithium-ion batteries have become ubiquitous in modern technology, including laptops, cell phones, and automobiles. A common problem in the battery field is quickly charging batteries while maintaining safe operation and limiting degradation. Slow charge times are a significant barrier to the widespread adoption of electric vehicles (EVs). Fully charging an EV battery pack can take several times longer than refilling the gasoline in an internal combustion engine vehicle. Advanced battery management systems (ABMS) that provide safe, fast, and reliable charging are critical to delivering maximum efficiency from batteries.

Conventional lithium-ion battery (dis)charge protocols involve constant or variable current, voltage, and power operating modes, which are standard experimental measurements. Correspondingly, many battery simulation tools offer options to evaluate these operating modes *in silico*.¹⁻⁴ Several articles performing optimal charging have demonstrated use cases for alternative operating modes, including constant temperature as a safety mechanism to prevent extreme temperatures,⁵⁻⁷ constant lithium plating overpotential to limit the rate of parasitic side reactions on the anode,⁸ and constant concentration to protect from lithium depletion and oversaturation.^{5,7,9} Online optimal charging studies often use model predictive control (MPC) with reformulated or reduced-order models that are more computationally efficient at the cost of greatly simplifying the physics.

This article proposes General Operating Modes (GOMs) for battery simulations that extend their abilities beyond the conventional current, voltage, and power operating modes. This framework allows for efficient and deterministic simulation of novel operating modes such as constant or variable temperature, lithium plating overpotential, mechanical stress, and electrolyte- and solid-phase concentrations/potentials. First, we provide a brief background on differential-algebraic equations (DAEs) and introduce GOMs. Simulations using the GOM have a similar computational cost as a constant current simulation, and battery models of all scales can use this framework by first appending a single algebraic equation to the governing equations and then solving the coupled system of DAEs. Second, we propose a strategy for simulating the mixed continuous-discrete (aka hybrid) solution of the optimal charging problem,

where “continuous” refers to the direct simulation of operating modes (e.g., constant current, voltage, power) and “discrete” refers to a transition between operating modes. The charging problem is solved in terms of its initial condition(s), constraint(s), and terminal objective(s) that removes all additional degrees of freedom from the problem when combined with the GOM. Third, we present case studies using three models of increasing complexity: a thin-film nickel hydroxide electrode model, a Single-Particle (SP) model with temperature dynamics, and a Porous Electrode Theory (PET) model with spatially varying temperature. Four optimal charging case studies are presented, which utilize novel operating modes, including constant potential, temperature, plating overpotential, and electrolyte/solid particle concentrations. Lastly, we discuss coding and numerical considerations when simulating models with GOMs. This article is an extension of the authors’ previous work¹⁰ with the addition of the thin-film and SP models, the analysis of suboptimality for the non-isothermal SP model, and the discussion on coding and numerical considerations.

Novel Battery Operating Modes

This Section describes the numerical implementation of the GOM, which permits direct simulation of novel operating modes (e.g., constant/variable temperature, plating overpotential) for lithium-ion batteries, which can be efficiently and deterministically computed for models of all scales.

Differential-algebraic equations (DAEs).—Systems of ordinary differential equations (ODEs) are commonplace in science and engineering to describe physical phenomena. In many physical systems, some governing equations (such as the conservation of charge) are *algebraic*. DAE solvers simultaneously solve coupled systems of differential and algebraic equations.

Battery models are usually described by a set of partial differential equations (PDEs), which are converted into a system of DAEs by the finite difference or finite volume method.^a DAEs can be specified in *fully implicit* form,

$$F(y(t), \dot{y}(t), t) = 0, \quad [1]$$

^zE-mail: braatz@mit.edu

^aSuch systems are also referred to as *descriptor* or *singular* systems in the literature.

or in mass matrix form,

$$M(t)\dot{y}(t) = g(y(t), t), \quad [2]$$

where y is the vector of states, \dot{y} is the derivative of y with respect to time t , F and g are vectors that describe the physicochemical phenomena, and M is the square mass matrix. At a particular time instant t^* , the DAE solver calculates the values of the time derivatives of the states, $\dot{y}(t^*)$, and the states, $y(t^*)$. ODEs are a special case of DAEs, and the DAEs 1 and 2 can be rewritten as explicit ODEs when the Jacobian F_y or the mass matrix M is nonsingular.^b

General Operating Modes (GOMs).—Battery simulation tools conventionally offer current, voltage, and power operating modes.^{1–3} When writing code for a battery model, it is common to begin with a model that accepts a parametric input for the current and then revise the system of equations to satisfy voltage and power operation. Redefining the modeling equations to accommodate each operating mode independently is time-consuming, may not be possible for implicit constraints, and fragments the model code.

The GOM concept expands the possible operating modes during simulation, permitting complex simulations such as constant/variable temperature, lithium plating overpotential, and electrolyte/solid concentrations. With the GOM, the battery governing equations are augmented with a single algebraic constraint that solves for the current, $I(t)$. Here, $I(t)$ is treated as an *algebraic state* in the modeling equations, which is found by simultaneously solving the governing equations and an additional algebraic constraint within a DAE solver. Generally, $I(t)$ is determined to satisfy the constraint

$$f(y, \dot{y}, t) = 0, \quad [3]$$

where $f(y, \dot{y}, t)$ is any user-specified function that is physically achievable.

Algebraic states (e.g., current, voltage, potentials) are determined by the residual between the algebraic state and an applied value,

$$\xi(y, \dot{y}, t) - \xi_{\text{app}}(y, \dot{y}, t) = 0, \quad [4]$$

where $\xi(y, \dot{y}, t)$ is a state or model output and $\xi_{\text{app}}(y, \dot{y}, t)$ is the desired value of ξ (which may be constant or a function of the time and/or states). For example, the expression for a constant current (CC) simulation is

$$I(t) - I_{\text{app}} = 0, \quad [5]$$

for an applied current I_{app} . Constant power (CP) is similarly defined as

$$I(t)V(t) - P_{\text{app}} = 0. \quad [6]$$

where P_{app} is the applied power defined by Ohm's law and the voltage $V(t)$ is the difference between the solid potentials at the electrode-current collector interfaces,

$$V(t) := \Phi_s(x, t)|_{x=L} - \Phi_s(x, t)|_{x=0}. \quad [7]$$

For the simple CC and CP examples, $I(t)$ can be solved analytically and inserted into the modeling equations, but this is not required under the GOM. Consider the constant voltage (CV) operating mode,

$$V(t) - V_{\text{app}} = 0. \quad [8]$$

In this case, $V(t)$ is an implicit function of $I(t)$, which cannot be solved analytically, but the algebraic constraint for $I(t)$ will still be satisfied by the DAE solver.

In contrast to algebraic states, differential states (e.g., concentration and temperature) are determined by a constraint on their

^b F_y is the Jacobian with respect to y , i.e., $\partial F/\partial y$.

derivative,

$$\frac{\partial \xi(y, \dot{y}, t)}{\partial t} - \Delta_t \xi_{\text{app}}(y, \dot{y}, t) = 0, \quad [9]$$

where $\Delta_t \xi_{\text{app}}(y, \dot{y}, t)$ is the desired rate of change of ξ . Constraints on differential terms are more restrictive than constraints on algebraic terms: the value of differential states at some time, t^* , is always fixed, but their rate of change as a function of time may change freely. The distinction between algebraic and differential terms is evident when fixing states to a constant: algebraic states are fixed by setting ξ_{app} of 4 to the desired value, while differential states are fixed by setting $\Delta_t \xi_{\text{app}}$ of 9 to zero given that the value of the differential state at t^* is already equal to the desired value. For example, the residual for the temperature derivative,

$$\frac{dT}{dt} - \Delta_t T_{\text{app}} = 0, \quad [10]$$

maintains a constant temperature (CT) operating mode fixed at $T(t^*)$ when the temperature rate of change, $\Delta_t T_{\text{app}}$, is set to zero.

Example operating modes are presented in the Case Studies Section for the thin-film electrode, SP, and PET models. Example GOM equations are summarized in Table I.

Mathematical Reformulation of Fast Charging Protocols

This Section outlines the framework of the hybrid solution for charging protocols of lithium-ion batteries.

Dynamic optimization.—Srinivasan et al.¹¹ describe methods for solving finite-time optimal control problems which allow for discrete transitions in the control input trajectory. The optimal control trajectory is parameterized as a combination of active *equality path constraints* where the states strictly follow along the arc of a specified bound, *singular arcs* where the sensitivity of the objective function is small,¹² *switching times* which denote the transition point between intervals, and *terminal objectives* that end the simulation. Analytical solutions were derived to satisfy the equality path constraints and singular arcs to solve single-input optimal control problems. Replacing optimization with analytical solutions that satisfy equality path constraints dramatically reduces the computational cost of solving the control problem. A limitation of the approach¹¹ is that deriving closed-form analytical expressions can be tedious or impossible for complex and nonlinear models.

Hybrid solution strategy.—Charging Li-ion batteries in a minimum amount of time while remaining within constraints is a common problem in the literature. Constraints (often based on heuristics) are chosen to ensure safe operation and to minimize degradation. The proposed framework has the same goals as in the numerical optimization-based approach to determining fast charging protocols but is distinctively different in its implementation. For specificity, consider a charging protocol formulated in terms of *optimizing* an objective function:

$$\min_{u(t), t \in [0, T_f]} J = \int_0^{T_f} \phi(y(t), u(t), t) dt, \quad [11]$$

subject to the constraints

$$u_{\text{lb}} \leq u(t) \leq u_{\text{ub}}, \quad [12]$$

$$y_{\text{lb}} \leq y(t) \leq y_{\text{ub}}, \quad [13]$$

where J is the control objective, ϕ is the cost function, u is the input to the system (for batteries, the current), T_f is the final time, and the subscripts lb and ub denote lower and upper bounds respectively. A typical objective function for the optimal charging problem is to

Table I. GOM equations to simulate various operating modes for the thin-film electrode, SP, and PET models.

Operating mode	Thin-film	Single-Particle	Porous Electrode Theory
Current	$I(t) - I_{app} = 0$	$I(t) - I_{app} = 0$	$I(t) - I_{app} = 0$
Voltage	—	$V(t) - V_{app} = 0$	$V(t) - V_{app} = 0$
Power	—	$I(t)V(t) - P_{app} = 0$	$I(t)V(t) - P_{app} = 0$
Potential	$\Phi(t) - \Phi_{app} = 0$	—	$\Phi(x, t) _{x^*} - \Phi_{app} = 0$
Ionic flux	$j(t) - j_{app} = 0$	$j(x, t) _{x^*} - j_{app} = 0$	$j(x, t) _{x^*} - j_{app} = 0$
Plating overpotential	—	—	$\eta_p(x, t) _{x^*} - \eta_{p,app} = 0$
Concentration rate of change	$\frac{dy}{dt} - \Delta_r y_{app} = 0$	$\frac{\partial c(x, t)}{\partial t} \Big _{x^*} - \Delta_r c_{app} = 0$	$\frac{\partial c(x, t)}{\partial t} \Big _{x^*} - \Delta_r c_{app} = 0$
Temperature rate of change	—	$\frac{dT}{dt} - \Delta_r T_{app} = 0$	$\frac{\partial T(x, t)}{\partial t} \Big _{x^*} - \Delta_r T_{app} = 0$

minimize the time required to reach some final State of Charge (SOC).

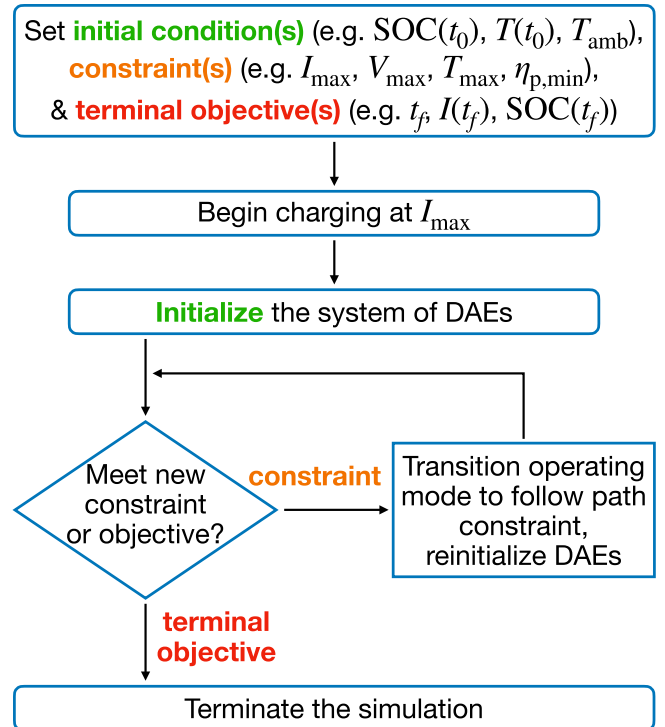
This article proposes an approach for determining fast-charging protocols that follows equality path constraints numerically instead of analytically. The critical insight is that, with the GOM, the charging trajectories do not need to be derived analytically since a relationship with current *can be stated and solved numerically within the DAE solver*. The flowchart in Fig. 1 describes the mixed continuous-discrete (aka hybrid) solution applied to the fast charging problem for lithium-ion batteries, where “continuous” refers to the direct simulation of operating modes (e.g., constant current, voltage, power) and “discrete” refers to a transition between operating modes. The first input to the system is always the same: maximize the current to charge as fast as possible. If the model encounters a new inequality constraint (e.g., $V(t) \leq V_{max}$) different from the active equality constraint during runtime, then the active constraint switches to enforce the new equality path constraint at the boundary (e.g., 8), and the system of DAEs is reinitialized with the updated GOM equation. This hybrid procedure finds the fast charging protocol deterministically defined by its initial condition(s), constraint(s), and terminal objective(s).

Several articles on fast charging are consistent with the above framework either explicitly or as a result of a control algorithm—the most well-known example is the constant current-constant voltage (CC-CV) charging protocol. Park et al.¹³ applied Pontryagin’s Minimum Principle to analytically derive optimal charging trajectories for an SP model with a Padé approximation in the solid particles, which were found to follow the same hybrid framework described above. Pathak et al.¹⁴ employ Proportional-Integral (PI) control and set-point tracking to enforce boundaries on states of the thin-film, SP, and reformulated P2D models. Mohtat et al.⁷ also followed a similar framework using a tuned PI controller to establish a CC-CV-CPo-C σ -CT protocol, where C σ is constant mechanical stress. Gains of the PI controller must be retuned to account for different set points (some of which are not experimentally observable, such as plating overpotential and mechanical stress) or model parameters.

Case Studies

This Section presents four case studies that simulate novel operating modes with the GOM (see the Novel Battery Operating Modes Section) using a simple thin-film electrode model, an SP model, and a PET model. The examples follow the hybrid fast charging framework (see the Mathematical Reformulation of Fast Charging Protocols Section).

The thin-film and PET models are simulated with the Julia programming language,¹⁵ and the SP model is simulated with MATLAB.¹⁶ Since Julia is a compiled language, the first evaluation of the model is slow. Reported evaluation times are after the first run. All tests are performed on a 2019 MacBook Pro 2.4 GHz 8-Core Intel i9 computer with 32 GB of RAM.


Figure 1. Flowchart for the mixed continuous-discrete (hybrid) solution to charging protocols.

Thin-film nickel hydroxide electrode model.—The galvanostatic charge of a thin-film nickel hydroxide electrode is described by the simple DAE system

$$\frac{dy}{dt} = \frac{j_1(t)W}{\rho VF}, \quad [14]$$

$$j_1(t) = 2i_{01} \left(1 - y(t) \exp \left(\frac{(\Phi(t) - \Phi_{eq,1})F}{2RT} \right) - y(t) \exp \left(-\frac{(\Phi(t) - \Phi_{eq,1})F}{2RT} \right) \right), \quad [15]$$

$$j_2(t) = i_{02} \left(\exp \left(\frac{(\Phi(t) - \Phi_{eq,2})F}{RT} \right) - \exp \left(-\frac{(\Phi(t) - \Phi_{eq,2})F}{RT} \right) \right), \quad [16]$$

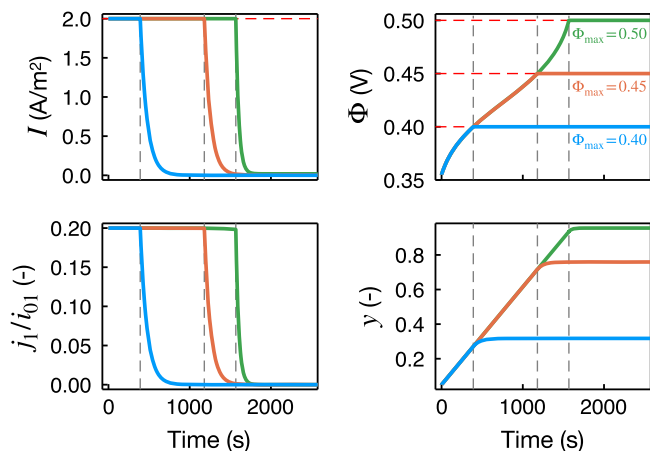


Figure 2. CC-C Φ charging protocol at three values of Φ_{\max} for the thin-film nickel hydroxide electrode model. The gray vertical lines indicate the transitions from constant current to constant Φ operating modes.

$$j_1(t) + j_2(t) - 10^{-5}I_{\text{app}} = 0, \quad [17]$$

where $y(t)$ is the mole fraction of nickel hydroxide, $\Phi(t)$ is the potential difference at the solid-liquid interface, and $j(t)$ is ionic flux, and the remaining parameters are listed in Table A1. In the standard CC formulation above, the applied current I_{app} is a parameter—with the GOM, we replace I_{app} with the time-varying state variable $I(t)$,

$$j_1(t) + j_2(t) - 10^{-5}I(t) = 0, \quad [18]$$

and append an additional algebraic equation to the governing equations which solves for $I(t)$ at every time instance. Even with this simple model, the GOM approach permits new operating modes such as constant/variable mole fraction, potential, and fluxes (see Table I). This model is simulated in Julia using the implicit DFBDF solver and static arrays, which are very fast for small systems of equations.

Case study I.—The goal is to quickly charge an electrode and enforce a maximum potential:

$$\begin{aligned} y(t_0) &= 0.350236 \\ I(t) &\leq 2 \text{ A/m}^2 \\ \Phi &\leq \Phi_{\max} \\ t_f &= 2, 500 \text{ s} \end{aligned} \quad [19]$$

where $\Phi_{\max} \in \{0.40 \text{ V}, 0.45 \text{ V}, 0.50 \text{ V}\}$. The CC operating mode is evaluated by simultaneously solving 5, 14–16, 18, which is equivalent to the standard formulation using I_{app} in 14–17. The algebraic constraint

$$\Phi(t) - \Phi_{\text{app}} = 0 \quad [20]$$

maintains a constant potential (C Φ) operating mode by simultaneously solving 14–16, 18, 20. While the standard formulation of the thin-film model is implicit and does not have an analytical solution for the states, the C Φ formulation does have an analytical solution (see A1–A5).

The charging protocols follow a similar trend for all Φ_{\max} (Fig. 2):

1. The initial input is the CC operating mode ($I_{\text{app}} = 2 \text{ A/m}^2$ in 5) at the upper bound to charge the cell as quickly as possible.
2. The input switches to the C Φ operating mode ($\Phi_{\text{app}} = \Phi_{\max}$ in 20) when the potentials reach the various Φ_{\max} values until the final time of 2500 s.

Starting with CC, $\Phi(t)$ and $y(t)$ increase monotonically until $\Phi(t) = \Phi_{\max}$ at various times. When the C Φ operating mode is activated, the current follows an exponential decay. By 2000 s, the model states approach steady state with a small but non-zero current.

A significant benefit of the GOM approach is that the analytical solution does not need to be derived, nor is its existence required—the C Φ expression 20 can be solved numerically along with the physical governing equations. During the C Φ operating mode, the analytical solutions for the states match the numerical solutions within the specified tolerances indicating that the GOM and the DAE solver are working correctly. With Julia, the average wall time to simulate each charging protocol is 103 μs .

Single-Particle (SP) model.—The SP model is a widely used reduced-order electrochemical model for simulating lithium-ion batteries.¹⁷ In each electrode, a single solid particle describes Fickian diffusion of lithium and interfacial reaction kinetics at the particle surface. Electrolyte dynamics are assumed uniform throughout the electrodes (in contrast to the pseudo-two-dimensional model described by PET in case studies III–IV). This article uses a modified SP model from Ref. 17 with temperature dynamics and spectral collocation in the solid particles. To support the GOM, the SP model was converted from a system of ODEs to a system of DAEs. The resulting system of DAEs has 40 equations: 20 Chebyshev node points were chosen to discretize each solid particle (19 equations in each section), 1 equation for temperature, and 1 equation for the GOM. This model is simulated in MATLAB using the implicit ode15i solver for a LiCoO₂ cell. The reader is referred to Ref. 17 for the complete set of governing equations and parameter values.

Case study II.—Degradation mechanisms in lithium-ion batteries¹⁸ are highly sensitive to temperature, so avoiding extreme temperatures is key to a long-lasting battery. Extreme temperatures are avoided by simulating a CT operating mode, where $\Delta_r T_{\text{app}}$ in 10 is set to zero.

The objective is to charge a cell to an SOC of 90% in the minimum amount of time under the constraints

$$\begin{aligned} \text{SOC}(t_0) &= 0\% \\ \text{SOC}(t_f) &= 90\% \\ T(t_0) &= 25 \text{ }^\circ\text{C} \\ T(t) &\leq T_{\max} \\ V(t) &\leq 4.2 \text{ V} \\ I(t) &\leq I_{\max} \end{aligned} \quad [21]$$

with an ambient temperature of 25 $^\circ\text{C}$.

First, we will analyze an example where $I_{\max} = 5\text{C}$ and $T_{\max} = 40 \text{ }^\circ\text{C}$. The resulting fast charging protocol for this problem (shown in Fig. 3) consists of four intervals:

1. The initial input is the CC operating mode ($I_{\text{app}} = 5\text{C}$ in 5) at the upper bound to charge the cell as quickly as possible.
2. The input switches to the CV operating mode ($V_{\text{app}} = 4.2 \text{ V}$ in 8) when the voltage reaches the maximum voltage.
3. The input switches to the CT operating mode ($\Delta_r T_{\text{app}} = 0 \text{ K/s}$ in 10) when the cell temperatures reaches 40 $^\circ\text{C}$.
4. The input again switches to the CV operating mode ($V_{\text{app}} = 4.2 \text{ V}$ in 8) when the voltage reaches the maximum voltage until the SOC hits its target of 90%.

The CC-CV-CT-CV protocol charges the cell from 0%–90% SOC in 1902.3 s. At 94.8 s, the operating mode transitions from the initial 5C charge to a short CV hold at 4.2 V. The cell temperature continues to rise until the maximum temperature of 40 $^\circ\text{C}$ after 164.0 s. At the CV to CT transition, the current falls dramatically from 4.5C to 3.9C to avoid crossing the temperature threshold. The nonlinearity of 10 and the dramatic change in current significantly

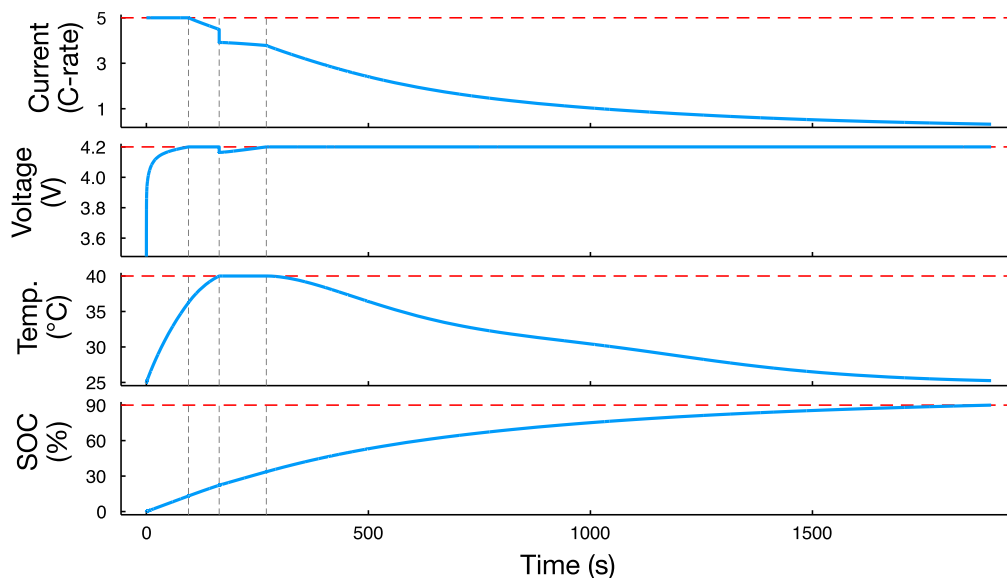


Figure 3. Fast charging results for a CC-CV-CT-CV protocol with the SP model.

increase the stiffness of the system of DAEs. Still, the solver can efficiently handle these changes using an adaptive time-stepping algorithm. After charging for an additional 106 s, the voltage again reaches 4.2 V and the CV hold is maintained until reaching the final SOC of 90%. In MATLAB, the wall time to simulate the SP model with 40 equations is 71 ms, which is comparable to a runtime of a CC simulation.

Park et al.¹³ applied PMP to an isothermal SP model with Padé approximation in the solid particles to show a *Bang-Ride* approach is globally optimal. As such, the search space for solutions to the optimal charging problem can be reduced to only the hybrid charging trajectories. These results imply that the proposed hybrid charging approach is globally optimal for the isothermal SP model.

The proposed approach can be suboptimal for the nonisothermal SP model. Figure 4 shows the total charge time and resulting protocols for the thermal SP model while varying I_{\max} and T_{\max} with 21. In most cases, the charge time decreases as the constraints become less restrictive when I_{\max} and T_{\max} increase; however, for $T_{\max} < 40$ °C, increasing I_{\max} can increase the charge time using the hybrid algorithm. For example, for $T_{\max} = 32$ °C, the charge time for maximum currents of 5C and 5.5C is 2124.8 and 2125.4 s, respectively, a 0.6 s increase in charge time for an increased C-rate. This shows that the hybrid algorithm can be suboptimal in some cases, at least to a small degree. The $I_{\max} = 5.5C$ protocol is suboptimal because the $I_{\max} = 5C$ protocol satisfies all constraints of the $I_{\max} = 5.5C$ protocol while charging slightly more quickly. Notably, this only occurs for increases in maximum current, $\partial t_f / \partial I_{\max} |_{\text{SOC}(t_f)=90\%} \in \mathbb{R}$, but increases in maximum temperature do not lead to greater charge times, $\partial t_f / \partial T_{\max} |_{\text{SOC}(t_f)=90\%} \leq 0$. The example in Fig. 4 with the highest amount of suboptimality is for a constant $T_{\max} = 30$ °C, where $I_{\max} = 3.97C$ results in a CC-CT-CV protocol which charges the most quickly in 2287.0 s and the CV-CT-CV protocol ($I_{\max} \geq 14.2C$) charges in 2293.4 s—a small 6.4 s or 0.28% increase in charge time. Having some degree of suboptimality is not a significant concern when the approach is used within a nonlinear model predictive control algorithm, as such algorithms intrinsically incorporate a feedback mechanism to correct for small deviations from global optimality at each sampling instance.¹⁹

When I_{\max} and T_{\max} are free parameters, six protocols arise from the hybrid charging algorithm. Figure 4 shows a complex relationship between the various charging protocols. For small values of I_{\max} , the current is not large enough to activate CV or CT charging, resulting in a single-step CC protocol. For large values of I_{\max} , the

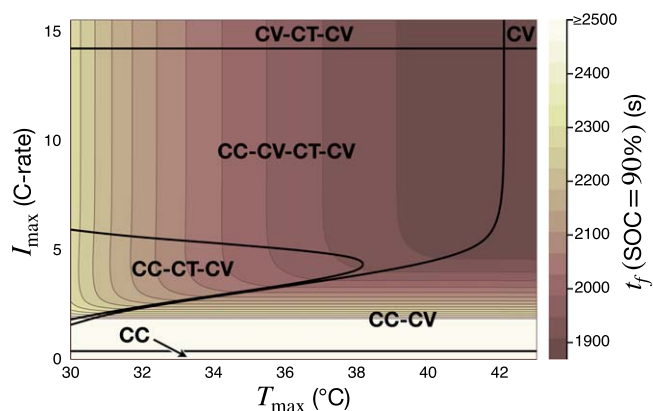


Figure 4. Total charge time with the SP model subject to the constraints in 21. Six charging protocols are possible when varying I_{\max} and T_{\max} . The color axis is cut off at 2500 s for visual clarity as I_{\max} approaches 0.

cell voltage quickly hits the upper bound of 4.2 V resulting in protocols such as CC-CV-CT-CV. At an initial applied C-rate of $I(t_0) = 14.2C$, the voltage instantaneously hits the upper bound and enters the CV mode, removing all initial CC steps where $I_{\max} \geq 14.2C$. The CC-CV-CT-CV region envelops the CC-CT-CV region. The single-step CV protocol, unconstrained by I_{\max} and T_{\max} , is the fastest charging protocol at 1870.0 s.

Porous Electrode Theory (PET) model.—In PET, each porous electrode has an electrically conductive solid phase in close contact with a liquid electrolyte.^{20–23} Lithium ions are dynamically transported between active particles in the electrolyte described by Fickian diffusion and Ohmic conduction. The two phases are coupled by interfacial electrochemical kinetics, typically modeled in the literature by Butler-Volmer kinetics but adaptable to Marcus theory. Solid-phase transport is assumed to be Fickian. The PET model is commonly referred to as being “pseudo-two-dimensional (P2D),” in which one dimension is the position between the two metal contact points on the opposite sides of the electrode-separator-electrode sandwich, and the second dimension is the distance from the center of a solid particle.

To simulate PET, this article uses PETLION,¹ which is an open-source high-performance computing implementation of the PET

model in Julia based on the finite volume method. The PETLION package on GitHub²⁴ has been updated to include all operating modes described in this article. Examples are provided online to show how a user can define new operating modes by specifying $f(y, \dot{y}, t)$ in 3. In all case studies, the model has 10 discretizations in the cathode, separator, anode, current collectors, and each solid particle for 351 total DAEs. The system of DAEs is solved using the IDA solver in SUNDIALS²⁵ with the KLU sparse linear solver²⁶ for a LiCoO₂ cell. The reader is referred to Ref. 3 for the complete set of governing equations and parameter values.

Case study III.—In addition to lithium-ion intercalation reactions, various side reactions occur in the cell which may cause the battery to degrade during charge. Anodic side reactions leading to lithium plating have been shown to occur when the lithium plating overpotential becomes negative.²⁷ The lithium plating overpotential is defined as

$$\eta_p(x, t) := \Phi_s(x, t) - \Phi_e(x, t), \quad [22]$$

where the equilibrium potential of the side reaction is usually assumed to be 0 V. During fast charging, the anodic lithium plating overpotential is minimized at the separator-anode interface ($x = L_n$). A constant lithium plating overpotential (CPo) at the lower bound is maintained by satisfying the constraint

$$\eta_p(x, t)|_{x=L_n} - \eta_{p,app} = 0, \quad [23]$$

where $\eta_{p,app}$ is the desired plating overpotential at the interface.

Consider a fast charging protocol with constraints to reduce degradation from lithium plating:

$$\begin{aligned} \text{SOC}(t_0) &= 0\% \\ \text{SOC}(t_f) &= 60\% \\ T(x, t_0) &= 30 \text{ }^\circ\text{C} \\ V(t) &\leq 4.1 \text{ V} \\ I(t) &\leq 4\text{C} \\ \eta_p(x, t)|_{x=L_n} &\geq 0 \text{ V} \end{aligned} \quad [24]$$

Following the hybrid charging framework of hybrid solution strategy subsection, the resulting CC-CPo-CV charge consists of three continuous intervals with two discrete transitions:

1. The initial input is the CC operating mode ($I_{app} = 4\text{C}$ in 5) at the upper bound to charge the cell as quickly as possible.
2. The input switches to the CPo operating mode ($\eta_{p,app} = 0 \text{ V}$ in 23) when the lithium plating overpotential at the separator-anode interface reaches the minimum bound to avoid degradative side reactions.
3. The input switches to the CV operating mode ($V_{app} = 4.1 \text{ V}$ in 8) when the voltage reaches its maximum bound until the SOC hits its target of 60%.

Figure 5 presents a comparison between the CC-CPo-CV protocol and a traditional CC-CV protocol which does not abide by the constraint on η_p . At $t = 325 \text{ s}$, the simulation enters the CPo operating mode and η_p is held exactly at $\eta_{p,app} = 0 \text{ V}$. Compared to CC-CV, the CC-CPo-CV protocol has a lower current and voltage during CPo to prevent the cell from charging too quickly and incurring degradation. Subsequently, the SOC(t) is slightly lower. After entering CV mode, the current is slightly higher than the CC-CV current for the same time point. The CC-CV and CC-CPo-CV protocols charge the cell to 60% SOC in 604.6 and 609.8 s respectively, which is a minor difference in charge time considering the significant advantage of avoiding the lithium plating side reactions with the CPo operating mode. An additional NMPC experiment subject to the constraints was compared to the CC-CV and CC-CPo-CV methods. The NMPC method used sequential quadratic programming (SQP) to minimize charge time with

constant current segments of sample time $\Delta t = 1 \text{ s}$. The NMPC results are visually identical to the CC-CPo-CV method. The simulation times for CC-CV and CC-CPo-CV are 8.4 and 14.7 ms, respectively. The 6.3 ms time increase in the CC-CPo-CV method is attributed to the CPo step, which makes the problem stiffer.

Case study IV.—Constraints on the solid active material and electrolyte protect from lithium depletion and oversaturation.⁹ The operating modes for constant electrolyte concentration (CCE) and constant solid surface concentration (CCss) are

$$\left. \frac{\partial c_{e,i}(x, t)}{\partial t} \right|_{x^*} - \Delta_t c_{e,i,app} = 0, \quad [25]$$

$$\left. \frac{\partial c_{s,i}^*(x, t)}{\partial t} \right|_{x^*} - \Delta_t c_{s,i,app}^* = 0, \quad [26]$$

respectively, where the subscript i refers to the section of the battery and $\Delta_t c_{e,i,app}$ and $\Delta_t c_{s,i,app}^*$ are the desired rate of change for electrolyte and solid surface concentrations, respectively. The GOM eqs. 25 and 26 must be evaluated at a particular position of the cell, x^* , as concentrations have large spatial variation. Upon reaching a maximum concentration constraint, the value of x^* for CCE and CCss operating modes are

$$\begin{aligned} x^* &= \arg \max_x c_{e,i}(x, t) \text{ and} \\ x^* &= \arg \max_x c_{s,i}^*(x, t), \end{aligned} \quad [27]$$

respectively (and likewise with $\arg \min_x$ for minimum constraints). These equations are general, but x^* is predictable for fast charging simulations: starting from rest, concentrations of the solid particle surface and electrolyte monotonically increase with x from the anode to the cathode. Constant concentrations at x^* are maintained by setting $\Delta_t c_{e,i,app} = 0$ or $\Delta_t c_{s,i,app}^* = 0$.

The objective is to charge a cell to an SOC of 80% in the minimum amount of time under the constraints:

$$\begin{aligned} \text{SOC}(t_0) &= 20\% \\ \text{SOC}(t_f) &= 80\% \\ c_{s,n}^*(x, t)/c_{s,n}^{\max} &\leq \theta_n^{\max} \\ c_e(x, t) &\geq 0.2 \text{ kmol/m}^3 \\ V(t) &\leq 4.1 \text{ V} \\ I(t) &\leq 4\text{C} \end{aligned} \quad [28]$$

where $c_{s,n}^*(x, t)/c_{s,n}^{\max}$ is the anodic solid particle surface concentration normalized by the maximum solid concentration and $\theta_n^{\max} = 0.85510$ is the maximum stoichiometry limit in the anode.

The results (Fig. 6) follow three discrete segments:

1. The initial input is the CC operating mode ($I_{app} = 4\text{C}$ in 5) at the upper bound to charge the cell as quickly as possible.
2. The input switches to the CCE operating mode ($\Delta_t c_{e,n,app} = 0 \text{ kmol/m}^3\text{s}$ in 25) when the minimum electrolyte concentration reaches 0.2 kmol/m^3 at the anode-current collector interface.
3. The input switches to the CCss operating mode ($\Delta_t c_{s,n,app}^* = 0 \text{ kmol/m}^3\text{s}$ in 26) when the normalized solid particle surface concentration in the anode reaches θ_n^{\max} . The simulation terminates upon reaching a final SOC of 80%.

The first transition (CC-CCE) occurs due to lithium depletion at the anode-current collector interface. At this transition, the current and voltage quickly drop to prevent $c_e(0, t)$ from falling below 0.2 kmol/m^3 before rising back up due to the high nonlinearity of the concentration dynamics. The effects of the transition are visible in the electrolyte concentration, where its spatial gradients immediately shift to ensure the concentration constraint is satisfied at the anode-

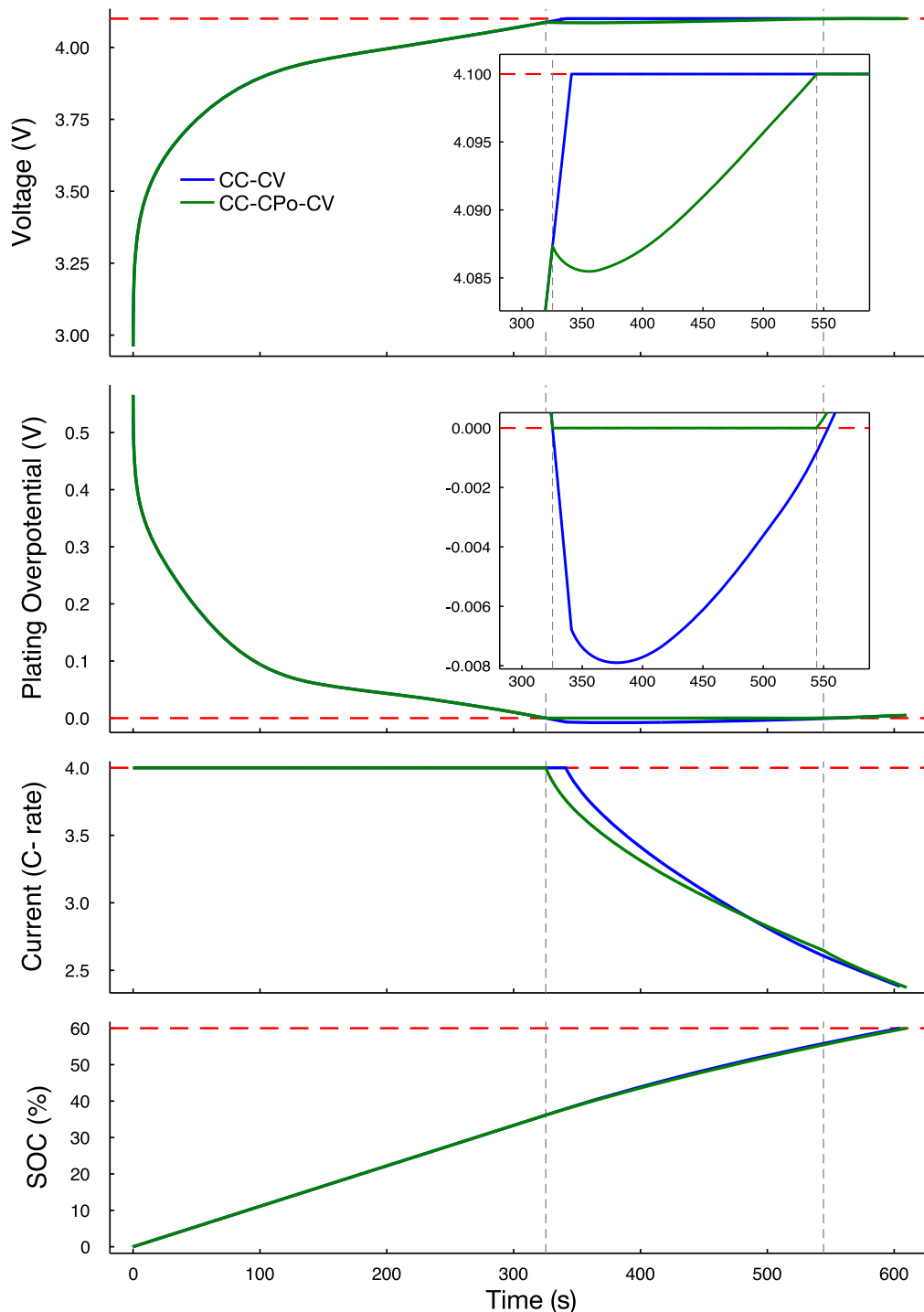


Figure 5. Fast charging results comparing a CC-CPo-CV and a CC-CV protocol with the PET model. The horizontal lines are the constraints, and the vertical lines denote the discrete switching times between operating modes for CC-CPo-CV.

current collector interface. A similar shift is seen in the solid surface concentration at the CCE-CCss transition to satisfy the solid surface constraint at the separator-anode interface. The second transition sees a drop in current and voltage, but the subsequent rise in current is much less pronounced in its speed and magnitude. With PETLION, the total evaluation time for the CC-CCE-CCss solution is 9.1 ms.

Coding and Numerical Considerations

GOM code implementation.— With the GOM, the model governing equations remain the same for all operating modes except for adding a single algebraic equation that solves for $I(t)$. One

method to differentiate between each operating mode in the code is with an “if” statement, which first defines the appropriate operating mode equation based on an input string and then evaluates that equation using the supplied value or function for ξ or $\Delta_i\xi$ (from 4 and 9 respectively). The code may also accept the user-defined expression in 3 as an input to the system. If the code uses an analytical Jacobian, the code must also involve a similar “if” statement for the row corresponding to the gradient of the GOM equation. If the Jacobian is sparse, its sparsity pattern must also be updated for each operating mode.

No feasible roots.—It is possible to specify a problem that only has a solution under certain conditions. If there are no feasible $y(t^*)$

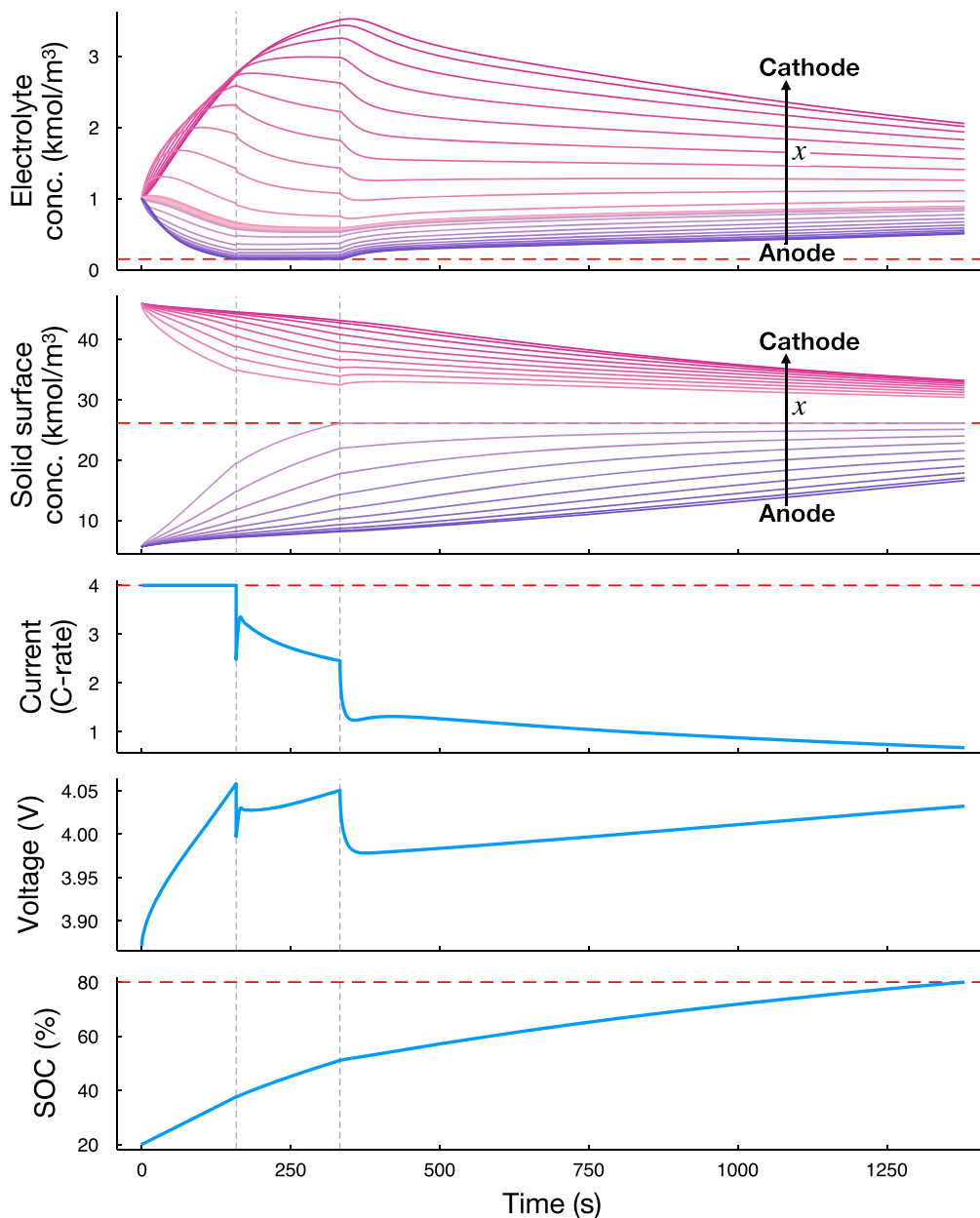


Figure 6. CC-CCe-CCss charging protocol with the PET model.

and $\dot{y}(t^*)$ to satisfy 3, then the solver will fail to converge. Consider a fast charging scenario using a constant temperature operating mode in 10. The minimum possible value of $dT/dt|_{t=t^*}$ occurs when the cell is at rest; the maximum value is unbounded as

$$\lim_{|I(t^*)| \rightarrow \infty} \frac{dT}{dt} \Big|_{t=t^*} = \infty. \quad [29]$$

Since dT/dt is continuous in $I(t^*)$, 10 has a feasible solution only if $\Delta_t T_{\text{app}} \geq dT/dt|_{I(t^*)=0}$.^c

Consistent DAE initialization.—A crucial part of simulating systems of DAEs is correctly initializing the algebraic and differential states at the start of the simulation (often using a nonlinear root-finding algorithm like Newton’s method). If the system cannot be properly initialized within the specified tolerances, the model may

fail to start or propagate errors from a poor initialization to further time points in the simulation.²⁸ Governing equations that form systems of ODEs (e.g., the SP model) may see a slight increase in computational cost with the GOM after being converted to a DAE system since DAE solvers can be slower than ODE solvers in some cases.

Event handling.—It is common to encounter events in battery simulations (e.g., exceeding the maximum temperature or voltage before the final time). Events can be handled *discretely*—instantly terminating the simulation after detecting a constraint violation—or *continuously*—finding the exact time when an event is violated. Continuous event handling is more computationally expensive than discrete event handling, but continuous event handling is required for accurate mixed continuous-discrete simulation.¹ Differential formulations of the GOM in 9 require that the simulation begins at a given initial value, which cannot be guaranteed with discrete event handling, but can be ensured with continuous event handling.

Increasing DAE index.—The DAE systems that simulate the thin-film, SP, and PET models in this article have a differential index

^cThe solution for 10 actually has two roots for I —one positive and one negative—since the limit in 29 is the *absolute value* of $I(t^*)$. If the initial guess for $I(t_0)$ is the correct sign when initializing the DAE, the nonlinear solver should converge to the root with the appropriate sign.

of 1. A user-defined algebraic equation to find $I(t)$ in 3 has the potential to increase the index of the system of equations which may not be solvable with standard DAE solvers.^{28–30} The approach in this article applies to higher index DAEs by reduction to index-1 DAEs by the dummy derivative method.³¹

Conclusions

This article presents General Operating Modes (GOMs), an approach to efficiently simulate novel operating modes for lithium-ion battery models of all scales. The GOM framework moves beyond the conventional current, voltage, and power operating modes to simulate new operating modes such as constant/variable temperature, plating overpotential, concentrations, and potentials regardless of model complexity or nonlinearity. The battery governing equations are augmented with a single algebraic constraint and solved as a coupled system of DAEs. The computational cost to simulate the novel operating modes is similar to that of a CC simulation for the same model. We present a flowchart for the mixed-continuous discrete (aka hybrid) solution to the fast charging problem. The solution uses the GOM to embed the solution of the control problem within the DAE solver, which is dependent only on the specified initial condition(s), constraint(s), and terminal objective (s). Case studies are presented that use the hybrid solution for fast charging for three models of increasing complexity: a thin-film electrode model, an SP model with temperature, and a PET model with spatially varying temperature. Considerations about the coding and numerical implementation of the GOM are detailed.

As discussed in case study III, the proposed approach results in a globally optimal charging protocol for the isothermal SP model. On the other hand, it is shown that a small amount of suboptimality can occur for the non-isothermal SP model. Some amount of suboptimality is acceptable within a nonlinear model predictive control algorithm as minor deviations from global optimality are corrected by feedback mechanisms. Although not of practical importance within the context of nonlinear model predictive control, characterizing the types of battery models for which the proposed hybrid approach produces a globally optimal charging protocol is of theoretical interest and a topic for future work.

Acknowledgments

This work was supported by the Toyota Research Institute through the D3BATT Center on Data-Driven-Design of Rechargeable Batteries.

Appendix

The standard formulation for the constant current, thin-film nickel hydroxide electrode model (see 14–17) is implicit and does not have an analytical solution. When the potential is fixed to a constant applied potential, Φ_{app} , the ODE for dy/dt is a linear differential equation with the analytical solution

$$y(t) = \frac{((a + 1/a)y(t_0) - a)e^{-(t-t_0)/\tau} + a}{a + 1/a}, \quad [A1]$$

for an initial mole fraction $y(t_0)$ where the constants a and τ are

$$a = \exp\left(\frac{(\Phi_{app} - \Phi_{eq,1})F}{2RT}\right) \text{ and } \tau = \frac{\rho VF}{2i_{01}W(a + 1/a)}. \quad [A2]$$

The analytical expressions for the remaining algebraic states are


$$j_1(t) = 2i_{01}((1 - y(t))a - y(t)/a), \quad [A3]$$

$$j_2 = i_{02}\left(\exp\left(\frac{(\Phi_{app} - \Phi_{eq,2})F}{RT}\right) - \exp\left(-\frac{(\Phi_{app} - \Phi_{eq,2})F}{RT}\right)\right), \quad [A4]$$

$$I(t) = 10^5(j_1(t) + j_2). \quad [A5]$$

ORCID

Marc D. Berliner  <https://orcid.org/0000-0002-2511-1853>

Richard D. Braatz  <https://orcid.org/0000-0003-4304-3484>

References

1. M. D. Berliner, D. A. Cogswell, M. Z. Bazant, and R. D. Braatz, *J. Electrochem. Soc.*, **168**, 090504 (2021).
2. V. Sulzer, S. G. Marquis, R. Timms, M. Robinson, and S. J. Chapman, *Journal of Open Research Software*, **9**, 14 (2021).
3. M. Torchio, L. Magni, R. B. Gopaluni, R. D. Braatz, and D. M. Raimondo, *J. Electrochem. Soc.*, **163**, A1192 (2016).
4. Introduction to COMSOL Multiphysics®, English, 1998, 158 pp.
5. C. Zou, C. Manzie, and D. Nešić, *IEEE/ASME Transactions on Mechatronics*, **23**, 947 (2018).
6. A. Pozzi, M. Torchio, R. D. Braatz, and D. M. Raimondo, *Journal of Power Sources*, **461**, 228133 (2020).
7. P. Mohtat, S. Pannala, V. Sulzer, J. B. Siegel, and A. G. Stefanopoulou, (2021), arXiv:2108.07833.
8. S. Kolluri, S. V. Aduru, M. Pathak, R. D. Braatz, and V. R. Subramanian, *J. Electrochem. Soc.*, **167**, 063505 (2020).
9. H. E. Perez, S. Dey, X. Hu, and S. J. Moura, *J. Electrochem. Soc.*, **164**, A1679 (2017).
10. M. D. Berliner, B. Jiang, D. A. Cogswell, M. Z. Bazant, and R. D. Braatz, “Fast charging of lithium-ion batteries by mathematical reformulation as mixed continuous-discrete simulation.” *Proceedings of the American Control Conference*, p. 5265 (2022), doi: 10.23919/ACC53348.2022.9867170.
11. B. Srinivasan, S. Palanki, and D. Bonvin, *Computers & Chemical Engineering*, **27**, 1 (2003).
12. M. Schlegel, K. Stockmann, T. Binder, and W. Marquardt, *Computers & Chemical Engineering*, **29**, 1731 (2005).
13. S. Park, D. Lee, H. J. Ahn, C. Tomlin, and S. Moura, “Optimal control of battery fast charging based-on Pontryagin’s Minimum Principle.” *Proceedings of the IEEE Conference on Decision and Control*, p. 3506 (2020), doi:10.1109/CDC42340.2020.9304409.
14. M. Pathak, S. Kolluri, and V. R. Subramanian, *J. Electrochem. Soc.*, **164**, A973 (2017).
15. J. Bezanon, A. Edelman, S. Karpinski, and V. B. Shah, *SIAM Review*, **59**, 65 (2017).
16. D. J. Higham and N. J. Higham, *MATLAB Guide* (SIAM, Philadelphia, PA) (2016).
17. A. M. Bizeray, J.-H. Kim, S. R. Duncan, and D. A. Howey, *IEEE Transactions on Control Systems Technology*, p. 1 (2018).
18. T. M. Bandhauer, S. Garimella, and T. F. Fuller, *J. Electrochem. Soc.*, **158**, R1–(2011).
19. F. Allgöwer and A. Zheng, *Nonlinear Model Predictive Control* (Birkhäuser) 26 (2012).
20. M. Doyle, T. F. Fuller, and J. Newman, *J. Electrochem. Soc.*, **140**, 1526 (1993).
21. J. Newman and W. Tiedemann, *AIChE J.*, **21**, 25 (1975).
22. T. F. Fuller, M. Doyle, and J. Newman, *J. Electrochem. Soc.*, **141**, 1 (1994).
23. T. F. Fuller, M. Doyle, and J. Newman, *J. Electrochem. Soc.*, **141**, 982 (1994).
24. M. D. Berliner and R. D. Braatz, *PETLION.jl* (2021), <https://github.com/MarcBerliner/PETLION.jl>.

Table A1. Parameters in the thin-film nickel hydroxide electrode model.⁸

Symbol	Value	Description
T	303.15 K	Temperature
$\Phi_{eq,1}$	0.420 V	Equilibrium potential
$\Phi_{eq,2}$	0.303 V	Equilibrium potential
W	92.7 g	Mass of active material
V	10^{-5} cm ³	Volume
i_{01}	10^{-4} A/cm ²	Exchange current density
i_{02}	10^{-10} A/cm ²	Exchange current density
ρ	3.4 g/cm ³	Density

25. A. C. Hindmarsh, P. N. Brown, K. E. Grant, S. L. Lee, R. Serban, D. E. Shumaker, and C. S. Woodward, *ACM Transactions on Mathematical Software (TOMS)*, **31**, 363 (2005).
26. T. A. Davis and E. Palamadai Natarajan, *ACM Transactions on Mathematical Software (TOMS)*, **37**, 1 (2010).
27. P. Kollmeyer, A. Hackl, and A. Emadi, "Li-ion battery model performance for automotive drive cycles with current pulse and EIS parameterization." *Proceedings of the IEEE Transportation Electrification Conference and Expo*, p. 486 (2017), doi:10.1109/ITEC.2017.7993319.
28. V. Ramadesigan, P. W. Northrop, S. De, S. Santhanagopalan, R. D. Braatz, and V. R. Subramanian, *J. Electrochem. Soc.*, **159**, R31 (2012).
29. P. I. Barton, R. J. Allgor, W. F. Feehery, and S. Galán, *Industrial & Engineering Chemistry Research*, **37**, 966 (1998).
30. K. E. Brenan, S. L. Campbell, and L. R. Petzold, *Numerical Solution of Initial-Value Problems in Differential-Algebraic Equations* (SIAM, Philadelphia, PA) (1995).
31. S. E. Mattsson and G. Söderlind, *SIAM Journal on Scientific Computing*, **14**, 677 (1993).